Energy Equip. Sys./ Vol. 6/No. 1/March 2018/ 69-87

ENERGY EQUIPSYS

Energy Equipment and Systems

http://energyequipsys.ut.ac.ir
www.energyequipsys.com

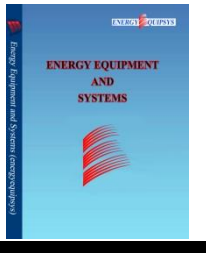

Xergy analysis and multiobjective optimization of a biomass gasification-based multigeneration system

Authors

Halimeh Rashidi [a]*
Jamshid Khorshidi [a]

[a] Faculty of Engineering, University of Hormozgan, Bandar Abbas, Iran

ABSTRACT

Biomass gasification is the process of converting biomass into a combustible gas suitable for use in boilers, engines, and turbines to produce combined cooling, heat, and power. This paper presents a detailed model of a biomass gasification system and designs a multigeneration energy system that uses the biomass gasification process for generating combined cooling, heat, and electricity. Energy and exergy analyses are first applied to evaluate the performance of the designed system. Next, the minimizing total cost rate and the maximizing exergy efficiency of the system are considered as two objective functions and a multiobjective optimization approach based on the differential evolution algorithm and the local unimodal sampling technique is developed to calculate the optimal values of the multigeneration system parameters. A parametric study is then carried out and the Pareto front curve is used to determine the trend of objective functions and assess the performance of the system. Furthermore, sensitivity analysis is employed to evaluate the effects of the design parameters on the objective functions. Simulation results are compared with two other multiobjective optimization algorithms and the effectiveness of the proposed method is verified by using various key performance indicators.

Article history:

Received : 19 September 2017
Accepted : 22 October 2017

Keywords: Multiobjective Optimization, Exergy Analysis, Pareto Front, Biomass Gasification, Differential Evolution Algorithm, Local Unimodal Sampling.

1. Introduction

Biomass is an alternative energy source which, unlike a fossil fuel, is carbon-neutral, widely available, and helps reduce waste and global warming. Since biomass is a renewable energy resource and is environment-friendly, it can be used to replace or reduce dependency on fossil fuels [1]. Hence, hybrid energy systems based on renewable energies, such as biomass for multigeneration purposes, are important for effective energy production and environment protection.

Biomass-based energy systems have been studied over many years by numerous researchers for various industrial applications. Recently, a number of studies have focused on biomass-based trigeneration and multigeneration systems.

Authors in [2] have designed a multigeneration system that is fuelled by gasified biomass and natural gas. They concluded that renewable energy is the source for reducing CO_2 and environmental impact. Performance assessment and the optimization of an integrated biomass energy system for multigeneration

* Corresponding author: Halimeh Rashidi
Faculty of Engineering, University of Hormozgan, Bandar Abbas, Iran
Email: halimeh_rashidi@yahoo.com

purposes have been conducted in [3], in which results have shown that the energy and the exergy efficiencies of the overall system are higher than the efficiencies of the individual biomass system. Energy and exergy analyses of a biomass based multigeneration system using an organic Rankine cycle (ORC) has been performed in [4], in which simulation results have shown that the maximum exergy efficiency of the ORC increases from 13 percent to 28 percent from a single generation to multigeneration. Authors in [5] have developed thermodynamic, energy, and exergy analyses on a biomass-based integrated system, in which they have investigated the effects of the design parameters on system operation. The simulation results reported in [5] illustrate that increasing the operation temperature of fuel cells cause more exergy destruction of the system in the fuel cell and the combustion chamber. Authors in [6] have developed energy and exergy of a combined cooling, heat and power (CCHP) system based on solar energy and biomass. The simulation results for the system used in [6], which includes the absorption chiller, heater, desalination system, biomass burner, and solar collector, show that the energy and the exergy efficiency are 61 and 7 percent, respectively. Reference [7] has presented an integrated system based on biomass energy, in which the effects of the various system parameters on energy and exergy efficiencies have been examined. The simulation results presented in [7] show that the energy and the exergy efficiencies are 66.5 and 39.7 percent, respectively. Authors in [8] have proposed an optimization model for biomass gasification based Building Combined Cooling, Heating and Power (BCHP) system. They have also calculated the most optimal scheme in terms of cost, energy consumption, steel consumption, and carbon dioxide emission. Authors in [9] have focused on modeling, simulation, and the economic analysis of the small-scale biomass CCHP system. The results presented in [9] show that the maximum efficiency and the best electricity price for the proposed system are as 85 percent and £87 / MWH, respectively. A CCHP system that includes a biomass gasifier, a double effect absorption refrigeration cycle, a HRSG, and a solid oxide fuel cell has been designed in [10] and its performance has been and compared with a CHP system. Authors of [10] have shown, using exergy and energy analysis, that the maximum exergy efficiency and CO_2 emission of the CCHP system are, respectively, significantly higher and lower than the same parameters of the CHP system. The results of the studies presented in [11] for a system that consists of three subsystems, i.e., a biomass gasification plant, a hydrogen liquefaction unit, and a solid oxide fuel cell/gas turbine (SOFC/GT), has shown that the SOFC/GT system provides considerably higher exergy efficiency in comparison to propulsion systems. Authors of [12] have studied the energy and exergy analysis of an integrated coal-based gasification system for hydrogen production and electric power generation, in which they have concluded that the energy and exergy efficiencies are 41 and 36.5 percent, respectively. A hybrid energy system for hydrogen production and electric power generation has been modeled in [13]. The model includes a photo voltaic array, wind turbines, an electrolyzer, a polymer electrolyte membrane fuel cell, a hydrogen tank, and a converter. The energy and the exergy analysis of the hybrid system have shown that the average energy and exergy efficiencies of the PV array are 13.31 and 14.26 percent, respectively; for the electrolyzer equipment, on the other hand, the average energy and exergy efficiencies are 59.68 and 60.26 percent; for the wind turbine, these values are 46 and 50.12 percent. The energy analysis of a solar-based biomass gasification system for hydrogen production has been presented in [14], in which three gasification processes have been studied. In the first gasification process, a gasification reactor has been selected along with a conventional water gas shift section and a pressure swing absorber. In the second gasification process, a gasification reactor, followed by an integrated membrane water gas shift reactor has been considered. In the third gasification process, a supercritical gasification reactor, followed by two flash separators and a pressure swing absorber have been selected. The results of the conducted simulations have shown that the optimal solar share of the second process is higher than the optimal solar share of the first process. Moreover, solar integration was not possible in the third process. Authors of [15] have presented exergy, energy, and the exergoeconomic analysis of a biomass-based hydrogen production system. Their analysis has shown that on the basis of the parameters used in their study, the cost of hydrogen produced by the circulating fluidized bed gasifier system is in the range of $1.59/kg to $5.37/kg. An energy production system that consists of biomass gasification as well as a fuel cell system has been studied in [16], in which the energy and exergy

analysis have shown that the effect of the steam biomass ratio on the hydrogen production efficiency is significant. A solar thermal system has been used in [17] as an energy source to supply the electrolyzer of the coupled hydrogen and solar energy system, in which a detailed model of the fuel cell and the thermal solar system have been studied. A multigeneration system that consists of geothermal and solar for generating electrical power, cooling, heating, hydrogen, and hot water for buildings has been presented in [18], in which energy and exergy analysis have been shown according to the internal parameters used in the study. The net cost of the optimized system is $476,000 and the levelized cost of electricity is $0.089/kWh.

The energy and exergy analysis of a geothermal power-based multigeneration energy production system conducted in [19] has shown that while geothermal water temperature rises, electrical power generation as well as the hydrogen production increase, but the hydrogen production cost decreases.

Reference [20] has developed a model for the designing, optimizing, and simulation of an energy system based on biomass gasification, which includes five configurations for power, heating, and cooling production. The results presented in [21] show that the exergy efficiency of the system is in the range of 18.9 to 23.2 percent. Energy and exergy analysis of a biomass-based energy system, which includes cooling, heating, and power cogeneration, has been presented in [22]. Energy, exergy, and economic analyses of the system show that the exergy efficiency is 28 percent, and the total destructed exergy of the biomass burner and the ORC evaporator are 55 and 38 percent, respectively.

Multigeneration systems based on renewable energies, such as biomass, potentially provide numerous benefits, such as higher efficiencies, reduced greenhouse gas emissions, reduced operating costs, and better use of resources. However, there are many design parameters that have significant effects on system performance, ranging from economic, thermodynamic, and environmental aspects. Hence, from the engineering application point of view, it is necessary apply optimization techniques to find the best values for the design parameters in order to improve system performance. The optimization process of a multigeneration energy system with many design parameters is a complicated and challenging task. Hence, the use of an efficient and global optimization algorithm is essential for the optimal design of such systems.

The employed methods for the optimization of multigeneration systems are generally categorized into classical methods and intelligent optimization algorithms. Classical optimization techniques cannot guarantee convergence with the global optimal solution when there are many design parameters [23]. In addition, according to the results presented in the literature, in complex and nonlinear optimization problems, such as multigeneration energy systems, intelligent optimization algorithms are superior to classical methods in finding the optimal solution [24]. As a result, in the field of multigeneration energy systems, certain researchers used evolutionary algorithms, such as the genetic algorithm and the particle swarm optimization technique [25–26] to find the optimum values for design parameters.

Single-objective optimization is not suitable for evaluating the performance of a multigeneration system because there are many factors that impact its performance from economic, thermodynamic, and environmental aspects. For example, in [27], for a multigeneration system, it has been shown that there is not an optimal condition where all the objective functions can reach their optimum values. For maximizing thermal efficiency and simultaneously minimizing the total cost rate of a multigeneration system, the elitist NSGA-II has been used in [3, 4]. A two-stage optimal design method, which uses the nondominated sorting genetic algorithm (NSGA-II) in the first stage and mixed-integer linear programming algorithm in the second stage, has been used for a CCHP system in [28]. A multiobjective PSO, called MOPSO, is used in [29] to obtain the maximum actual annual benefit and exergy efficiency of a trigeneration system. A multiobjective function, based on thermodynamic, economic, and environmental aspects, has been selected in [30] and a MOPSO algorithm has been used to optimize a CCHP system. Although a literature review shows that evolutionary algorithms, especially GA and PSO algorithms, provide quite good results in the field of multigeneration system optimization in order to fill the existing gap in the multiobjective optimization of a biomass gasifier-based multigeneration system and also increase the variety of available tools, other alternatives of optimization techniques shall also be taken into consideration.

This paper presents a detailed model of a biomass gasification system, designs a multigeneration system, and determines the best operating condition using multiobjective optimization techniques. Major highlights of this study are as follows:

- To model a multigeneration system consisting of a biomass combustor, an ORC, a double-effect absorption chiller, and a desalination unit.
- To perform exergy and exergoeconomic analyses of this multigeneration system.
- To propose and apply a new multiobjective optimization algorithm based on differential evolution (DE) and the local unimodal sampling (LUS) technique.
- To derive a closed-form expression for the Pareto optimal points curve to provide aid for the optimal design of the multigeneration system.
- To perform sensitivity analyses to evaluate the effects of the design parameters on the objective functions.
- To select the final optimum design point by using a fuzzy clustering-based decision-making method.
- To compare the performance of the proposed multiobjective optimization algorithm with other well-known intelligent optimization methods.
- To compare the comprehensive thermodynamic modeling, exergy analyses, and the environmental impact assessments of the system under study with other multigeneration systems.

The rest of this paper is organized as follows: The multigeneration energy system along with its thermodynamic modeling and analysis are described in Section 2. Exergy, energy, and economic analysis of the system are presented in Sections 3 and 4. Section 5 presents the proposed multiobjective optimization technique. The simulation results and the effects of the design parameters on the system performance analysis are shown in the Sections 6 and 7, respectively. The conclusions are provided in Section 8.

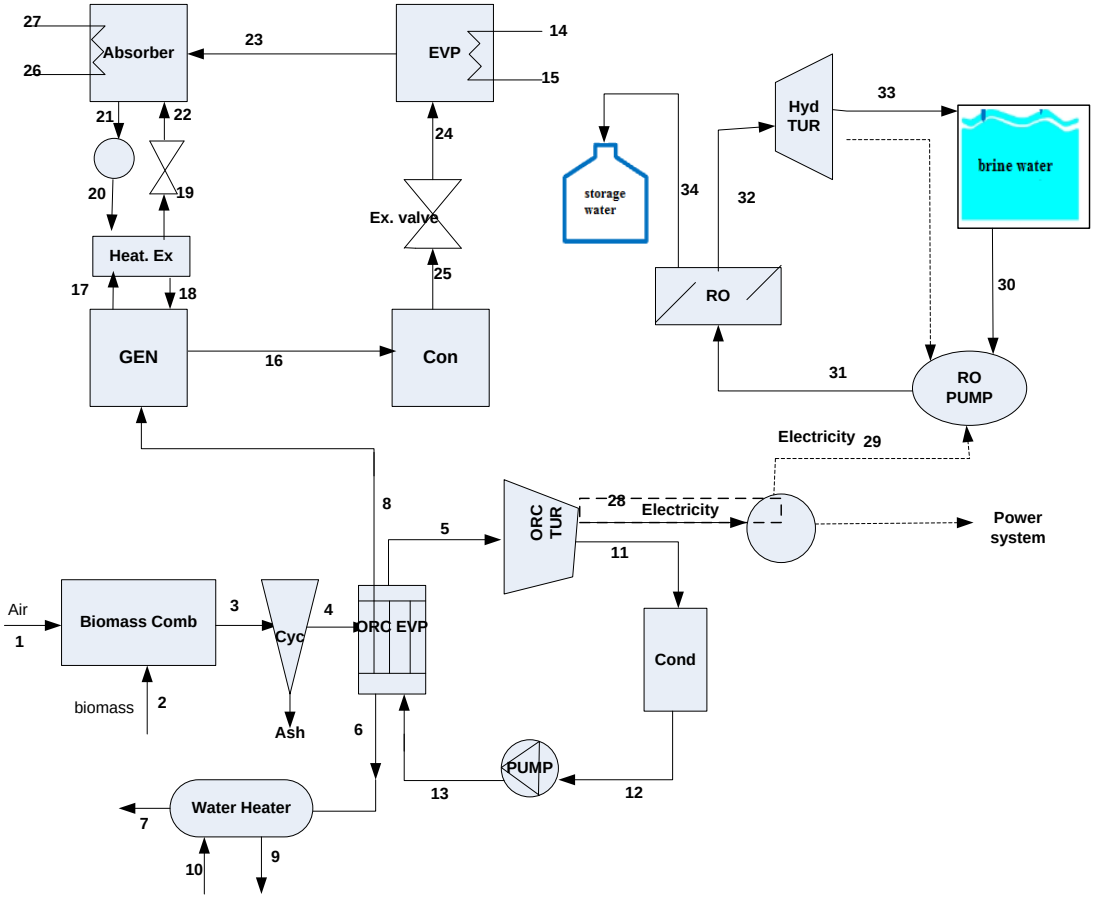

Fig. 1. Schematic diagram of the multigeneration system based on biomass gasification.

2. Assumption and system description

Figure 1 shows the schematic diagram of a biomass gasification-based multigeneration system. Such a system, which comprises a biomass fired hot air gas turbine, can be used when there is a simultaneous demand for electricity, heating, cooling, fresh water, and hot water. In this system, the synthesis gas produced via biomass gasification mixes with air in a combustion chamber and produces combustion products at 1450 K. Hot flue gas, after leaving the biomass combustion chamber, enters a cyclone to remove ash and then enters an ORC evaporator to produce steam. The steam is then used to derive the ORC turbine and generate electricity. The electricity is used to supply the power system and also derive RO desalination plant to produce fresh water. As the hot flue gas leaving the evaporator still has enough energy, it can be used in the water heater for producing hot water. Some of the hot flue gas that leaves the ORC evaporator is used to run the absorption chiller.

3. Thermodynamic modeling and analysis

For thermodynamic modeling, the multigeneration energy system that is described in Fig. 1 is divided into the following four subsystems: 1) biomass combustor, 2) ORC and domestic water heater, 3) absorption chiller, and 4) reverse osmosis desalination unit. The relevant energy equations of the system, shown in Fig. 1, are described in the following sections.

3.1. Biomass combustion

Biomass enters the combustor at Point 2 and air enters at Point 1. The gasification of biomass can be presented by the following reaction [3]:

$$C_x H_y O_z + \omega H_2O + \lambda\left(O_2 + 3.76N_2\right) \rightarrow aCO_2 + bH_2O + cN_2 \quad (1)$$

, where ω is the amount of water in biomass that is obtained from the equation below:

$$\omega = \frac{\dot{m}_{biomass} \times MC}{18\left(1-MC\right)} \quad (2)$$

The molar mass flow rate of biomass can be expressed as follows:

$$\dot{n}_{C_xH_yO_z} = \frac{\dot{m}_{biomass}}{M_{C_xH_yO_z}} \quad (3)$$

(a, b, c, and λ) in the right hand side of Eq.(1) are calculated by the mass balance of carbon, hydrogen, and oxygen as shown below:

$$a = x\ , b = \frac{y+2\omega}{2}\ , c = \frac{79}{21}\lambda, \lambda = \frac{2a+b-\omega-z}{2} \quad (4)$$

To find the chemical exergy at the inlet and the outlet of the combustion chamber, the following equation is obtained by writing the first law of thermodynamic for this process and ignoring the changes in potential energy and kinetic energy [4] as follows:

$$\bar{h}_{C_xH_yO_z} + \omega\bar{h}_{H_2O} + \lambda\bar{h}_{O_2} + 3.76\lambda\bar{h}_{N_2} = a\bar{h}_{CO_2} + b\bar{h}_{H_2O} + c\bar{h}_{N_2} \quad (5)$$

$$\bar{h}_{C_xH_yO_z} = x\bar{h}_{CO_2} + \left(\frac{y}{2}\right)\bar{h}_{H_2O} + \overline{LHV}_{biomass} M_{C_xH_yO_z} \quad (6)$$

The LHV biomass byproduct that is unknown here can be found by using the following equations [26, 27]:

$$\overline{LHV}_{biomass} = HHV_{biomass} - 226.04y - 25.82\omega \quad (7)$$

$$HHV_{biomass} = 338.3x + 1443\left(y - \frac{z}{8}\right) + 94.2\omega \quad (8)$$

Input energy to the system is defined as below:

$$Q_{biomass} = \left(\frac{\dot{n}_{C_xH_yO_z} M_{C_xH_yO_z}}{1000}\right)\overline{LHV}_{biomass} + \left(\dot{m}_{fuel}\right)\overline{LHV}_{CH_4} \quad (9)$$

3.2. Organic rankine cycle

The ORC is normally used for recovering energy from low-grade heat. As shown in Fig. 1, gases produced from the combustion of synthesis gas enter the evaporator and operate the ORC system. Applying thermodynamic law on each component will result in the following equation [31]. The equations describing the behavior of different parts of the ORC are shown as follows:

$$\dot{Q} + \sum \dot{m}_i h_i = \dot{W} + \sum \dot{m}_o h_o \quad (10)$$

Evaporator:

The energy balance equation for the evaporator is shown below.

$$\dot{m}_4 h_4 + \dot{m}_7 h_7 = \dot{m}_8 h_8 + \dot{m}_6 h_6 \quad (11)$$

Since, pinch point temperature is an important parameter to calculate the gas temperature leaving the evaporator, the following equation is used to define pinch point temperature:

$$T_{Pinch,Evap} = T_8 - T_7 \quad (12)$$

Turbine:

Energy balance for the ORC turbine yields the following relation [19]:

$$\eta_{Turbin} = \frac{\dot{W}_{Turbin,act}}{\dot{W}_{Turbin,isen}} \quad (13)$$

Energy balance for the control volume around the pump is described below [16] as follows:

$$\dot{W}_{pump} = \dot{m}_{in}\left(h_{out} - h_{in}\right) \quad (14)$$

The energy balance for control volume around the condenser is expressed as follows:

$$\dot{m}_9 h_9 = \dot{Q}_{cond} + \dot{m}_{10} h_{10} \quad (15)$$

$$\dot{Q}_{cond} = \dot{m}_{cooling}\left(h_{cooling,out} - h_{cooling,in}\right) \quad (16)$$

3.3. Model of water heater

Hot air that leaves the evaporator enters the water heater. Energy balance for the water heater will result in the following equation:

$$\dot{m}_{in} C_{p,g}\left(T_{in} - T_{out}\right) = \dot{m}_w\left(h_{w,in} - h_{w,out}\right) \quad (17)$$

3.4. Model of the RO desalination unit

The main components of an RO system include a high pressure pump, membrane separation units, and an energy recuperation system. In this paper, a standard RO unit with the following mass and energy-balancing equation is used [5]:

$$\dot{W}_{net} = b_n\left(\dot{W}_{pump} - \dot{W}_{turbin}\right) \quad (18)$$

where b_n is the number of trains, which is 7 in this study. $\dot{W}_{pump}$ and $\dot{W}_{turbin}$, which are work rate interaction of the RO pump and the hydro turbine, are defined as follows [6]:

$$\dot{W}_{Turbin} = \frac{\Delta P \dot{m}_{Fw} \eta_{turbin}}{\rho_{Fw}} \quad (19)$$

$$\dot{W}_{pump} = \frac{\Delta P \dot{m}_{BW}}{\eta_{pump}\rho_{BW}} \quad (20)$$

In the above equations, ΔP is the trans-membrane pressure, and η_{pump} and η_{turbin} are the efficiencies of the RO pump and the hydro turbine, respectively. The rate of fresh water flow $\dot{m}_{FW}$ is related to the rate of brain water, which is defined as follows [6]:

$$\dot{m}_{\mathrm{FW}} = \frac{\dot{m}_{\mathrm{BW}}}{RR} \quad (21)$$

The equation of the trans-membrane is shown as follows:

$$\Delta P = J_w k_m + \Delta\pi\ , \quad (22)$$

here, k_m is the membrane permeability resistance and J_w is the volumetric permeate flow rate as shown below:

$$J_w = \frac{\dot{m}_{\mathrm{FW}}}{\rho_{FW} nA}\ ,\ k_m = 8.03\times10^{-11}\frac{m^2 s}{kgPa} \quad (23)$$

In the above equation, n is the total number of membranes, ρ_{FW} is density of fresh water, and A is the membrane area. $\Delta\pi$, which is the osmotic pressure of the trans-membrane, is defined below [5].

$$\Delta\pi = 805.1\times10^5 C_W R \quad (24)$$

C_W, which is the membrane wall concentration, is expressed as follows:

$$C_W = \frac{e^{\left(\frac{J_W}{k}\right)} x_{12}}{e^{\left(\frac{J_W}{k}\right)}\left(1-R\right)+R} \quad (25)$$

where R is the membrane rejection coefficient and k is the mass transfer coefficient as shown below.

$$k = 0.04 Re^{0.75} Sc^{0.33}\frac{D_s}{d} \quad (26)$$

here, D_s is the diffusivity, d is the feed channel thickness, and SC is the Schmidt number as shown below.

$$SC = \frac{\mu}{\rho D_s} \quad (27)$$

3.5. Absorption Chiller

This sub-system is used for air conditioning and supplying the cooling load of the system. Applying mass conversion, and the first and the second laws of thermodynamics on each component of the absorption chiller, assuming steady state and steady flow, will result in the following equations:

$$\sum \dot{m}_i = \sum \dot{m}_O \quad , \quad \sum (\dot{m}x)_i = \sum (\dot{m}x)_O \tag{28}$$

$$\dot{Q} - \dot{W} = \sum \dot{m}_o h_o - \sum \dot{m}_i h_i \tag{29}$$

$$\dot{Q}_{cooling} = \dot{m}(h_{out} - h_{in}) \tag{30}$$

3.6. Exergy Analysis

Exergy analysis is an efficient tool for analyzing and improving industrial processes. Considering the steady state condition and applying the exergy balance equation will result in the following equation [27]:

$$\sum \dot{m}_{in} ex_{in} + \dot{E}x_Q = \sum \dot{m}_{out} ex_{out} + \dot{E}x_w + \dot{E}x_D \tag{31}$$

where $\dot{E}x$ is the exergy rate, $\dot{E}x_Q$, $\dot{E}x_w$, $\dot{E}x_D$ are the exergy rate of heat transfer crossing the boundary of the control volume, exergy rate associated with shaft work, and exergy destruction respectively; ex is the specific flow exergy of the process.

$$\dot{E}x_Q = \dot{Q}\left(1 - \frac{T_0}{T_i}\right), \ \dot{E}x_w = \dot{W} \tag{32}$$

$$ex = ex_{ke} + ex_{po} + ex_{ph} + ex_{ch} \tag{33}$$

The exergy of a substance (ex) is normally divided into four parts. These are physical, chemical, kinetic, and potential exergy. Since the speeds are relatively slow and the elevation changes are small in this study, the kinetic and the potential exergies are assumed to be negligible.

$$e_{x,ph} = (h - h_0) - T_0 (S - S_0) \tag{34}$$

$$ex_{ch} = \left[\sum_{i=1}^{n} x_i ex_i^{ch} + \bar{R} T_0 \sum_{i=1}^{n} x_i ln(x_i) \right] \tag{35}$$

For calculating the chemical exergy of the ammonia-water solution in the absorption chiller, the following equation is used [32]:

$$ex_{sol}^{ch} = \frac{x}{M_{NH_3}} \overset{\circ}{ex}_{NH_3} + \frac{1-x}{M_{H_2O}} \overset{\circ}{ex}_{H_2O} \tag{36}$$

$\overset{\circ}{ex}_{NH_3}$ and $\overset{\circ}{ex}_{H_2O}$ are the chemical exergies of ammonia and water, respectively. In accordance, the exergy of the system will be as follows [32]:

$$\Psi_{power} = \frac{\dot{W}_{net,ORC}}{\dot{E}_{x,biomass}} \tag{37}$$

$$\Psi_{CHP} = \frac{\dot{W}_{net,ORC} + \dot{E}_{x,heating}}{\dot{E}_{x,biomass}} \tag{38}$$

$$\Psi_{multi} = \frac{\dot{W}_{net,ORC} + \dot{E}_{x,heating} + \dot{E}_{x,cooling,chiller} + \dot{E}_{x,HW} + \dot{E}_{x,FW}}{\dot{E}_{x,biomass}} \tag{39}$$

$$\dot{E}_{x,heating} = \dot{Q}_{cond}\left(1 - \frac{T_0}{T_{cond}}\right), \ \dot{E}_{x,cooling} = \dot{Q}_{cooling}\left(\frac{T_0 - T_{Evap}}{T_{Evap}}\right) \tag{40}$$

$$\dot{E}_{x,HW} = \dot{m}_{HW}(h_{in} - h_{0ut}) - T_0(S_{in} - S_{out}) \tag{41}$$

$$\dot{E}x_{biomass} = \dot{m}_{biomass} \beta \overline{LHV}_{mois} \tag{42}$$

$$\beta = \frac{1.0414 + 0.0177\left(\frac{H}{C}\right) - 0.3328\left(\frac{O}{C}\right)\left\{1 + 0.0537\left(\frac{H}{C}\right)\right\}}{1 - 0.4021\left(\frac{O}{C}\right)} \tag{43}$$

Table 1 summarizes the equations related to exergy destruction and efficiency for the different components of the system.

3.7. Economic Analysis

The cost function of each component and the total cost of the system are obtained by using economic analysis. One can obtain the cost rate by using the equations presented in [5] as follows:

$$\dot{Z} = \frac{Z_k CRF \varphi}{N \times 3600} \tag{44}$$

Z_k is the purchase cost of the component and CRF is the capital recovery factor. N is the number of hours the component works per year and φ is the maintenance factor; N = 8000 hours and φ = 1.06, respectively, in this paper.

CRF is obtained by using the following equation [4]:

$$CRF = \frac{i \times (1+i)^n}{(1+i)^n - 1} \tag{45}$$

where i is the interest rate which is 12 percent and n is the number of operating years, which is 20 years in this paper. The cost rates of the environmental impact and fuel cost are expressed as follows [27]:

$$\dot{C}_{env} = C_{co_2} \dot{m}_{co_2} \ , \dot{C}_f = C_f \dot{m}_f LHV \tag{46}$$

The objective functions are exergy efficiency, which should be maximized, and the total product cost rate, which should be minimized. The total cost rate is [30] as follows:

$$\dot{C}_{tot} = \sum \dot{Z}_K + \dot{C}_{env} \tag{47}$$

where $\dot{Z}_K$ is the purchase cost of the components explained before. Table 2 shows the chosen values for the economic analysis of the system.

Table 1. Components exergy destruction of multigeneration system.

Components	Exergy Efficiency	Exergy Destruction
Biomass combustion chamber	$\Psi_{biomass} = \frac{\dot{E}_{x_1} + \dot{E}_{x_2}}{\dot{E}_{x_3}}$	$\dot{E}_{x_{D,E,Comb}} = \dot{E}_{x_1} + \dot{E}_{x_2} - \dot{E}_{x_3}$
ORC evaporator	$\Psi_{Evp} = \frac{\dot{E}_{x_4} + \dot{E}_{x_{13}} - \dot{E}_{x_6}}{\dot{E}_{x_5} + \dot{E}_{x_8}}$	$\dot{E}_{x_{D,E,Evap}} = \dot{E}_{x_4} + \dot{E}_{x_{13}} - \dot{E}_{x_5} - \dot{E}_{x_6} - \dot{E}_{x_8}$
ORC turbine	$\Psi_{Turbin} = \frac{\dot{W}_{Turbin}}{\dot{E}_{x,5} - \dot{E}_{x,11}}$	$\dot{E}_{x,D,Turbin} = \dot{E}_{x,5} + \dot{W}_{Turbin} - \dot{E}_{x,11}$
ORC Condenser	$\Psi_{cond} = \frac{\dot{E}_{x,11} - \dot{E}_{x,12}}{\dot{Q}_{cond}}$	$\dot{E}_{x,D,cond} = \dot{E}_{x,11} - \dot{Q}_{cond} - \dot{E}_{x,12}$
ORC Pump	$\Psi_{pump} = \frac{\dot{E}_{x,12} - \dot{E}_{x,13}}{\dot{W}_{Pump}}$	$\dot{E}_{x,D,Pump} = \dot{E}_{x,12} - \dot{W}_{Pump} - \dot{E}_{x,13}$
Water Heater	$\Psi_{W,Heater} = \frac{\dot{E}_{x_6} - \dot{E}_{x_7}}{\dot{E}_{x_{10}} - \dot{E}_{x_7}}$	$\dot{E}_{x,WH} = \dot{E}_{x_6} + \dot{E}_{x_{10}} - \dot{E}_{x_7} - \dot{E}_{x_9}$
Evaporator	$\Psi_{Evp} = \frac{\dot{E}_{x,24} - \dot{E}_{x,23}}{\dot{E}_{x,14} - \dot{E}_{x,15}}$	$\dot{E}_{x,D,Evp} = \dot{E}_{x,24} + \dot{E}_{x,14} - \dot{E}_{x,15} - \dot{E}_{x,23}$
Absorber	$\Psi_{Abs} = \frac{\dot{E}_{x_{22}} - \dot{E}_{x_{21}}}{\dot{E}_{x_{26}} - \dot{E}_{x_{27}}}$	$\dot{E}_{x_{D,E,Abs}} = \dot{E}_{x_{22}} + \dot{E}_{x_{26}} - \dot{E}_{x_{18}} - \dot{E}_{x_{21}}$
Expansion valve		$\dot{E}_{x_{D,E,evalve}} = \dot{E}_{x_{19}} + \dot{E}_{x_{25}} - \dot{E}_{x_{22}} - \dot{E}_{x_{24}}$
Pump		$\dot{E}_{x_{D,E,Pump}} = \dot{E}_{x_{21}} + \dot{W}_{Pump} - \dot{E}_{x_{20}}$
Heat exchanger		$\dot{E}_{x_{D,E,Hexch}} = \dot{E}_{x_{20}} + \dot{E}_{x_{17}} - \dot{E}_{x_{18}} - \dot{E}_{x_{19}}$
Absorber Generator		$\dot{E}_{x_{D,E,Gen}} = \dot{E}_{x_8} + \dot{E}_{x_{17}} - \dot{E}_{x_{18}} - \dot{E}_{x_{16}}$
Condenser		$\dot{E}_{x_{D,E,Cond}} = \dot{E}_{x_{16}} - \dot{E}_{x_{25}}$
RO pump		$\dot{E}_{x,D,RO\,Pump} = \dot{E}_{x,30} + \dot{W}_{pump} - \dot{E}_{x,31}$
RO desalination unit		$\dot{E}_{x,D,RO} = \dot{E}_{x,31} - \dot{E}_{x,32} - \dot{E}_{x,34}$
RO turbine		$\dot{E}_{x,D,RO\,Turbin} = \dot{E}_{x,32} - \dot{W}_{Turbin} - \dot{E}_{x,33}$

Table 2. Cost functions of the multigeneration system [4, 5, 27, 31, and 32]

Components	Cost	Definition
Biomass combustion chamber and evaporator	$Z_{combustion}(\$) = 740\left(\dot{m}_g h_3\right)^{0.8} exp\left(\frac{0.01P_6 - 2}{14.29}\right) exp\left(\frac{T_6 - 350}{446}\right)$	$\dot{m}_g$ is the flue gas mass flow rate
ORC Turbine	$Z_{Turbin}(\$) = 4750\dot{W}_{Turbin}^{0.75}$	$\dot{W}_T$ is the power generated by the turbine
Generator	$Z_T(\$) = 60\dot{W}_T^{0.95}$	$\dot{W}_T$ is the power generated by the turbine
ORC Condenser	$Z_{cond}(\$) = 516.62A_{cond}^{0.6}$ $A_{cond} = \frac{\dot{Q}_{cond}}{U_{cond}\Delta T_{ln}}$, $U_{cond} = 0.15$	U_{cond} is the overall heat transfer coefficien
ORC Pump	$Z_{Pump}(\$) = 200\dot{W}_{Pump}^{0.65}$	$\dot{W}_{pump}$ is the rate of pump work
Water Heater	$Z_{HW}(\$) = 0.3m_{HW}$	m_{HW} is mass of hot water production
Desalination Plant	$Z_{RO}(\$) = 0.98m^3$	m is the mass of fresh water
Absorption Chiller	$Z_{chiller}(\$) = \left(\dot{Q}_{Evap}\right)^{0.67}$	$\dot{Q}_{Evap}$ is the cooling load in absorption chiller

4. Multiobjective Optimization

In order to determine the optimal design parameters for the multigeneration system described in previous sections, a multiobjective optimization method based on the DE algorithm and the LUS technique are introduced. In the subsequent sections, the details of the proposed optimization algorithm and the design parameters are introduced.

4.1. DE Algorithm

The DE algorithm is an intelligent optimization method that starts with an initial random population consisting of the NP vectors $X_i, i = 1,2,\dots,NP$. For a d-dimensional problem, each vector i is represented by d variables as expressed by $X_i = [x_{i1}, x_{i2}, \dots, x_{id}]$, in which d is the number of decision variables. After initialization, these vectors are evolved by mutation and recombination operations to generate a mutant vector V_i with respect to each individual X_i. Many mutation strategies are available in the literature [33]. The classical strategy, which is "DE/rand/1", is presented below.

$$V_i = X_{r1} + F \times \left(X_{r2} - X_{r3}\right) \quad X_{r1} \neq X_{r2} \neq X_{r3} \neq X_i \qquad (48)$$

, where r_1, r_2, and r_3 are random integers within the range $[1, NP]$ and F is a scale factor in the range $(0, 2)$. After mutation, the crossover operator is applied to each pair of the target vector X_i and its corresponding mutant vector V_i to produce a trial vector $U_i = [u_{i1}, u_{i2}, \dots, u_{id}]$. In DE, the most commonly used crossover is the uniform crossover, which is defined as shown below [33].

$$u_{ij} = \begin{cases} v_{ij} & if\ rand < CR\ or\ j = l \\ x_{ij} & otherwise \end{cases} \qquad (49)$$

where u_{ij}, v_{ij}, and x_{ij} are the jth dimensional components of the vectors U_i, V_i, and X_i, respectively. CR is the predefined crossover probability, which is usually set to a fixed value in the range (0, 1). l is an integer number that is randomly chosen from the index set {1, 2,..., d} and is used to ensure that the trial vector U_i contains at least one parameter from the mutant vector V_i. After the crossover, the objective values of all the trial vectors are evaluated; thereafter, a selection mechanism is employed to select the population for the next generation. To perform this operation, the objective function of each trial vector U_i is compared to the objective of its corresponding target vector X_i in the current population. If the trial vector U_i gets a better objective function value than the target vector X_i, the trial vector will replace its corresponding target vector; otherwise, the current target vector is retained. In a minimization problem, this selection scheme is described as follows:

$$X_i^* = \begin{cases} U_i & if\ \ f(U_i) \leq f(X_i) \\ X_i & otherwise \end{cases} \qquad (50)$$

where $f(x)$ is the objective of a solution x and X_i^* is the parent vector used to replace the target vector in the next generation. The pseudo code of the DE algorithm is shown in Table 3.

Table 3. Pseudo code for DE Algorithm.

Objective function $f(X_i)$, $X_i = [x_{i1}, x_{i2}, \dots, x_{id}]$
1: Generate the initial population $P = [X_1, X_2, \dots, X_{NP}]$ randomly (NP individuals in d dimensions)
2: Repeat
3: For $i = 1$ to NP perform the operation
4: Select randomly $r1, r2, r3 \in [1, NP]$, $r1 \neq r2 \neq r3 \neq i$
5: Compute a mutant vector V_i by using the Eq. (48)
6: Create the trial vector U_i by the crossover of V_i and X_i by using Eq. (49)
7: If $f(U_i) < f(X_i)$, then $X_i = U_i$
8: Endif
9: Endfor
10: Until stopping condition is met.

4.2. Parameter Tuning of the DE algorithm

The successful implementation of DE depends on the proper selection of its control parameters. Factors that impact the performance of DE are the crossover rate CR, the scale factor F, and the population size NP. There is no agreement in the literature on how to optimally select these factors. For example, in [34], start with $F = 0.5$ and $CR = 0.1$ as good initial values have been suggested. However, as larger CR results in faster convergence, to check for a quick solution, trying $CR = 0.9$ or $CR = 1$ have been proposed. Authors in [35], based on several experimental analyses, have suggested $F = 0.2$ and CR in the range of [0.5 and 0.9] as good initial values. In [34], it has been concluded that $F = 0.9$ is a good compromise between the convergence speed and the convergence probability. Moreover, as CR depends on the nature of the optimization problem, reference [36] has suggested choosing CR in the range of 0.9 and 1 for non-separable and multimodal objective functions, and choosing CR in the range of 0 and 0.2 for separable objective functions. Reference [37] has suggested considering the nature of the problem and using sensitivity analysis for selecting the best CR value. Moreover, ElQuliti and Mohamed [37] have examined the correlation between F and CR by using some sample values and have concluded that a higher number of successes and failures occurred when $CR = 0.5$ and $CR = 1$, respectively. In [38–39], a self-adaptive SDE algorithm has been proposed, in which F is self-adapted by using a mutation rule similar to the mutation operator in the basic DE. As there is no fixed rule for the optimal selection of DE parameters and the optimal combination of these parameters may change based on desired accuracy and computational resources, in order to overcome the aforementioned drawbacks and also to avoid the tuning of parameters by the trial-and-error procedure, the LUS method described in next section is used in this paper for finding out the optimal values of the DE parameters.

4.3. LUS Algorithm

LUS uses sampling as well as a search-range through iteration methods to detect the best choice out of the tuning parameters for the optimization algorithms [40]. For each of the tuning parameters, LUS starts with a search range and then decreases it iteratively until the optimal value is reached. The search range is defined as $D = (D_1, D_2, \dots, D_n)$ where n is the total number of parameters to be optimized [41]. For example, in the DE algorithm, as there are four tuning parameters (i.e., CR, F, NP, and $MaxGen$),); $n = 4$. The initial search range is defined for each of the tuning parameters based on the upper and the lower boundaries $b_{up} = (b_{up1}, b_{up2}, \dots, b_{upn})$ and $b_{low} = (b_{low1}, b_{low2}, \dots, b_{lown})$.

$$D_i = b_{up,i} - b_{down,i} \tag{51}$$

Firstly, the optimal solution s is defined as $s = (s_1, s_2, \dots, s_n)$. Next, at $t = 0$, the value of each parameter is initialized to uniformly distribute random numbers as shown below [42].

$$s \sim U\left(b_{low}, b_{up}\right) \tag{52}$$

Then, the objective function is evaluated for the s values defined above. After that, a new set of DE parameters s_{new} is generated as shown below.

$$s_{new} = s + a \tag{53}$$

where $a = (a_1, a_2, \ldots, a_n)$ is a vector of uniformly distributed random values inside the search range D, ; i.e., $a \sim (-D, D)$.

Now, s_{new} is used to calculate the new fitness value. If this new fitness value is better than the initial fitness value, s is changed to $s = s_{new}$, ; otherwise, as shown below, the search range D is decreased for all the dimensions by multiplying with a factor q to determine a new set of parameters s_{new} [41].

$$D = qD \tag{54}$$

The decrease factor q is defined as the Eq.(55):

$$q = 2^{-\beta/n} \tag{55}$$

where β is a user-defined behavior parameter and n is the number of DE parameters that are being optimized.

The aforementioned process is repeated until the maximal number of iterations $maxEval$ for LUS algorithm is reached or until accuracy, for the generated set of weights, is 100 percent [40]. The pseudo code of the LUS algorithm [41] and the structure of the meta-optimization algorithm for DE are shown in Tables 4 and 5, respectively.

5. Multiobjective Optimization Problem

Multiobjective optimization problems (MOP) include several conflicting objective functions that should be simultaneously optimized. The outputs of the algorithms that optimize multiobjective problems are a set of nondominated solutions known as Pareto-optimal solutions. If X_1 and X_2 are two different solutions, X_1 dominates X_2 when no other solution can be found to dominate X_1 by using the definition of Pareto dominance as shown below [43].

$$\begin{cases} \forall i \in \{1,2,\ldots,n\}, F_i(X_1) \le F_i(X_2) \\ \exists j \in \{1,2,\ldots,n\}, F_j(X_1) < F_j(X_2) \end{cases} \tag{56}$$

where n is the number of objective functions. For a given MOP, the Pareto front $\mathcal{PF}^*$ is a set of vectors of the objective functions that are obtained by using the vectors of the design variables in the Pareto set P^*:

$$\mathcal{PF}^* = \{F_1(X), F_2(X), \ldots, F_n(X) \mid X \in P^*\} \tag{57}$$

where $P^* = \{X \in \Omega \mid \nexists X' \in \Omega : F(X') < F(X)\}$.

Table 4. Pseudo Code for the LUS algorithm [40].

1	Procedure LUS
2	Set $q \leftarrow 2^{-\beta/n}$
3	For dimension $j \epsilon \{1,2, \ldots, n\}$ ***do***
4	Set $s_j \sim U(lower\ Boundry\ j, upper\ Boundry\ j)$
5	Set $D_j \leftarrow \lvert upper\ Boundry\ j - lower\ Boundry\ j \rvert$
6	While $eval < maxEval\ and\ fitness > acceptFitness$ ***do***
7	**Set** $a_j \sim U(-D_j, D_j)$
8	**Set** $y_j \leftarrow s_j + a_j$
9	**If** $f(y_j) < f(s_j)$ **then**
10	**Set** $s_j \leftarrow y_j$
11	**Else**
12	**Set** $D_j \leftarrow q.D_j$

Table 5. Pseudo Code of LUS Based DE Algorithm

- Select DE parameters randomly and initialize LUS.
- Iterate LUS using the following steps:
- Among all earlier obtained set of DE parameters, select the most suitable parameter according to LUS optimization methodology.
- Calculate the key performance indicators to define how good the selected set of DE parameters is.
- Discard this new set of DE parameters if the calculated key performance indicators do not show improvements; otherwise, retain it.

The unique capability of DE and other intelligent optimization algorithms is that they can find multiple solutions in one single simulation run. However, the original MOP scheme has to be modified before it can be solved by using intelligent optimization algorithms. The proposed multiobjective DE algorithm is explained in the following section.

5.1. Multiobjective DE Algorithm

The MODE archives both dominated and nondominated solutions. Hence, an algorithm is needed to update the archived solutions and search for the solution which dominates other solutions. For performing this task, the ε-dominance method is used in this paper. In this method, the size of the final external archive depends on the ε value, which is normally a user-defined parameter. This method is briefly described in the section below.

5.2. Archive Updating

The first step involves checking whether solutions are feasible or not. A solution is considered feasible if it fulfills all constraints. The next step is to check whether a feasible solution is dominated by other solutions or not. The nondominated feasible solutions are then stored in the archive list. During this process, if any of the archived solutions are dominated by other solutions, then, the dominated solution solutions will be removed from the archive list. If there are not enough places for storing all the feasible solutions, a grid-based and ε-dominance method will be used in the archiving process. In this method, the dimension of the space will be equal to the number of objectives. Each dimension is divided into several boxes with a ε-to-ε size, such that each box contains one or more solutions. If the solutions inside a box are dominated by other boxes, the box, along with its solutions, will be removed. In the end, each box should hold only one solution. If a box has more than one solution, the solution at a lesser distance from the left corner of the box will remain and the others will be removed [44]. This will assure us that at the end of process that the retained solutions are nondominated feasible solutions.

Similar to a single objective DE algorithm, in which the trial vector replaces the target vector if the trial vector is better than target vector, in multiobjective DE, the target vector is replaced by the trial vector if the trial vector dominates the target vector [45]. However, if neither trial nor target vectors are dominated, crowding distance is applied to specify the less crowded distance as the new target vector for the next generation. For calculating crowding distance, the population is sorted in ascending order, based on the values of the objective functions. Then, boundary solutions (i.e., solutions with the highest and the lowest values) of each objective function are set to an infinite distance value and the remaining solutions (i.e., intermediate solutions) are set to the absolute normalized difference of two adjacent solutions. This process is repeated for all the objective functions and the overall crowding distance value is calculated as the sum of the individual distance values of each objective as shown below.

$$CD_i = \frac{1}{n}\sum_{j=1}^{n}\frac{f_i(k+1)-f_i(k-1)}{f_i^{max}-f_i^{min}}, \quad i = 2,\ldots,n-1 \tag{58}$$

, where CD_i is the ith individual crowding distance value and f_i is the ith objective function. From the above equation, it is observed that the CD is the mean value of Euclidean distance.

In order to illustrate the efficiency and the robustness of the proposed MODE algorithm, the algorithm is tested on the multigeneration system described in the previous sections. Moreover, the algorithm has been compared with two well-known multiobjective optimization algorithms called NSGAII [46] and MOPSO [47].

5.3. Decision Variables

The decision variables are selected from design parameters according to their impact on objective functions. In this paper, eight parameters have been selected as decision variables; these include evaporator temperature (T_{Evap}), pump efficiency (η_{pump}), pump inlet temperature (T_{pump}), evaporator pinch point temperature (T_{PP}), ORC turbine inlet pressure ($P_{ORC,Tur}$), ORC turbine inlet temperature ($T_{ORC,Tur}$), turbine efficiency (η_{Turbin}), and biomass flow rate ($\dot{m}_{biomass}$). The upper and the lower limits of these parameters are also shown in Table 6 [4].

5.4. Model Validation

The main part of the modeling exercise is related to the synthesis of the gas generation

Table 6. Characteristic parameters of the system.

Components	Constraints
Evaporator temperature	$275\ °K < T_{EVP} < 279°K$
Pump efficiency	$\eta_{pump} < 0.9$
Inlet pump temperature	T_{pump}<388°K
Evaporator pinch point temperature	283°K<T_{PP}< 308°K
ORC turbine inlet pressure	$1500\ Kpa < P_{ORC,Tur} < 3000Kpa$
ORC turbine inlet temperature	593°K <$T_{ORC,Tur}$<673°K
Turbine efficiency	$\eta_{Turbin} < 0.9$
Biomass flow rate	$0.2 < \dot{m}_{biomass} < 0.4$

section. Model validation is performed by comparing the synthesis gas composition with the compositions reported in the literature. Table 7 summarizes the synthesis gas composition obtained from the model presented in this paper and the synthesis gas composition reported in [48] as the results of experimental tests and synthesis gas composition reported in [49] as the results of conducted simulations. As observable from Table 7, compositions are close to each other and the proposed model accurately predicts the compositions.6. Optimization Results from the Proposed Model. In this section, the feasibility and the adequacy of the proposed MODE approach have been evaluated in the multigeneration system problem proposed in the previous sections. The settings for meta-optimization are explained hereafter. First, the range and the possible values of the DE parameters are chosen as follows:

$NP \in \{1,2,\ldots,200\}$, $MaxGen \in \{1,2,\ldots,300\}$,

$CR \in [0,1]$, $F \in [0,2]$

Then, LUS is performed trying to find the optimal choice of the DE parameters. After that, the objective values of a given choice of the DE parameters are computed. LUS has a number of iterations; out of these, 20 iterations are chosen. Using the above settings, the best performing parameters found for the DE method are as follows:

$NP = 23$, $MaxGen = 267$, $CR = 0.8246$,

$F = 0.4039$

The Pareto frontier solutions for the MODE, MOPSO, and NSGA-II optimization algorithms are shown in Fig. 2.

To show the effectiveness of the MODE optimization algorithm, its performance is measured and compared with the MOPSO and the NSGA-II optimization algorithms; two indices named generational distance defined in [45] as convergence metric and spread defined in [46] as diversity metric. To that end, a weighted metric combining the generational distance metric, *GD*, and the spread metric Δ, suggested in [47], is used and the best nondominated Pareto front obtained from the combined Pareto fronts of 20 independent runs of each algorithm for 300 generations are used to calculate the metrics as follows:

$W = w_1 GD + w_2 \Delta$

with $w_1 + w_2 = 1$

Smaller Δ refers to better diversity and smaller *GD* refers to better convergence. Hence, the algorithm with smaller *W* has better convergence and diversity ability.

Table 8 shows the weighted convergence and diversity metrics (*W*), assuming that *w1 = w2*. From this table, it is observed that performance of MODE is better than the NSGA-II and the MOPSO algorithms in terms of convergence as well as diversity. The solutions given by MODE have much better diversity than the other two algorithms because of the better diversity maintenance strategy of MODE. Moreover, the proposed MODE has a better distributing ability that helps convergence.

The Pareto curve, obtained using the proposed MODE algorithm for both objective functions, i.e., exergy efficiency and system cost, when the decision variables vary in their respective limits, is shown in Fig. 2. From this figure, it is observed that when the exergy efficiency increases, the total system cost also increases. Point *A* on the curve is the optimal solution when only the system cost is considered and the exergy efficiency is ignored. Point *C* on the curve is the optimal solution when only the exergy efficiency is considered and the system cost is ignored.

Table 7. Summarizes synthesis gas composition.

Composition	Value (%)	Lab results[48]	Duta [49]
Hydrogen (H_2)	17.6	17	18.03
Carbon monoxide (CO)	20.08	18.4	18.51
Carbon dioxide (CO_2)	10.78	10.6	11.43
Methane (CH_4)	1.13	1.3	0.11
Nitrogen (N_2)	50.42	52.7	51.92
Moisture content in biomass	16%	16%	16%

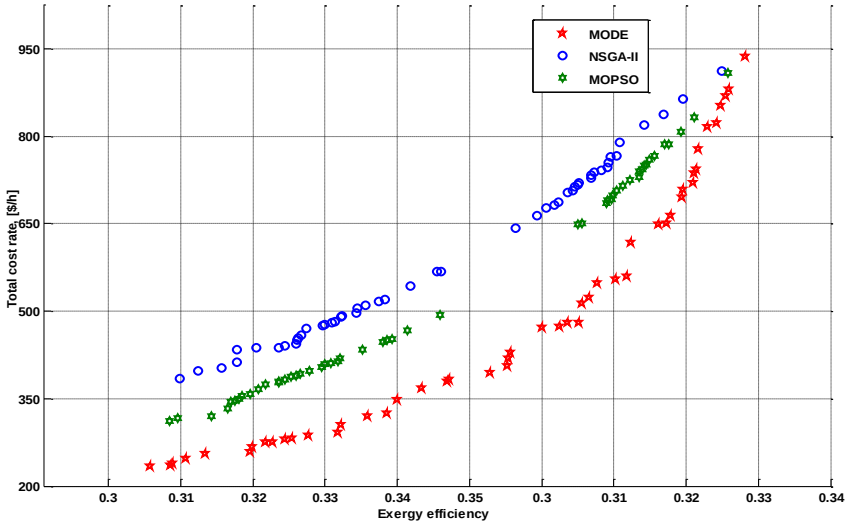

Fig. 2. Two-dimensional Pareto-optimal front.

Table 8. Performance metrics for three multiobjective optimization algorithms.

	Generational Distance			Spread			Weighted Metric		
	MODE	MOPSO	NSGA-II	MODE	MOPSO	NSGA-II	MODE	MOPSO	NSGA-II
Mean	0.00054	0.00063	0.00074	0.16507	0.25643	0.49576	0.53137	0.68429	1.0000
SD	0.00015	0.00017	0.00016	0.02431	0.04653	0.06362	0.63223	0.86568	0.97058
Min	0.00034	0.00041	0.00051	0.15159	0.32874	0.31372	0.56385	0.90196	0.97715
Max	0.00117	0.00127	0.00121	0.23438	0.59437	0.63065	0.64644	0.97123	0.97637

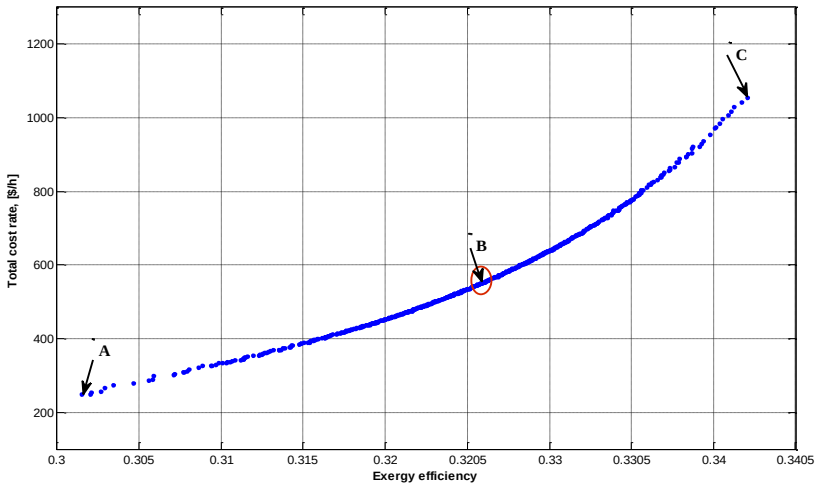

Fig. 3. Best trade-off values for the objective functions using proposed MODE.

As both objective functions cannot be simultaneously optimized, as shown in Fig. 3, the ideal solution is not on the Pareto curve. Although all the points on the Pareto curve are optimal solutions, the closest point to the ideal solution may be considered as the final optimal solution. Hence, the selection of the optimal solution depends on the preferences and the criteria of the decision maker. In this paper, the fuzzy decision making mechanism [50] is implemented to find out the best compromised solution. The linear membership value μ_i^j is initially calculated for the *ith* objective of the *jth* member, f_i^j, in the archive list using Eq.(61)

$$\mu_i^j = \begin{cases} 0 & f_i^j > f_i^{max} \\ \dfrac{f_i^{max} - f_i^j}{f_i^{max} - f_i^{min}} & f_i^{min} \le f_i^j \le f_i^{max} \\ 1 & f_i^j < f_i^{min} \end{cases} \quad (61)$$

, where f_i^{min} and f_i^{max} are the lower and the upper portions of the *ith* objective function. After that, a fuzzy decision-making approach is implemented as follows:

$$\mu^j = \frac{\sum_{i=1}^{n} \sigma_i \mu_i^j}{\sum_{j=1}^{M} \sum_{i=1}^{n} \sigma_i \mu_i^j} \quad (62)$$

, where M is the number of non-dominated solutions and μ^j is the membership function value of the non-dominated solution j. Then, the Pareto solution that obtains the maximum value of $\mu^j$is chosen as the compromised solution. In the above equation, σ_i is the desired weighting factor of the i^{th} objective function. It is worth mentioning that $\sigma_i \geq 0$ and $\sum_{i=1}^{n} \sigma_i = 1$. According to the above mechanism, Point B is selected as the best compromised solution. As observable, while moving from Point B toward Point C, the cost function increases and while moving from Point B toward A, the exergy efficiency reduces. Hence, it may be concluded that Point B is the closest point to the ideal solution from the exergy efficiency as well as the system cost point of view.

To find a relation between the exergy efficiency and the system cost rate, the curve shown in Fig. 3 has been fitted on optimal solutions resulting from multiobjective optimization. Moreover, a formula valid for the 30 to 34 percent range of exergy efficiency is defined for the fitted curve. This formula that can be used for estimating the optimal exergy efficiency as a function of the total system cost is shown in Eq.(63).

$$\dot{C}_{total} = 553.4e^{-\left(\frac{\varphi-0.347}{0.0156}\right)^2} + 604.9e^{-\left(\frac{\varphi-0.341}{0.0409}\right)^2} \quad (63)$$

Table 9 summarizes the values of the design parameters for the two critical Points *A* and *C* as well as the obtained compromised Solution *B*.

Table 10 shows certain characteristics of the system. As observable from this table, from Point *A* to Point *C,* both objective functions, i.e., the total cost rate and the exergy efficiency increase. As expressed before, Point *A* is preferred when the total cost rate is the sole objective function and Point *C* is the ideal solution when the exergy efficiency is the sole objective function. However, Point *B* shows better results for both objective functions. Other thermodynamic characteristics also confirm this choice. For instance, from Point *B* to *C*, the total exergy destruction rate decreases when the exergy efficiency increases.

7. Sensitivity Analysis

Sensitivity analysis is normally performed to study the impact of the important parameters on the system performance. The effects of the design parameters on both the objective function exergy efficiency (EE) and the total cost rate (TCR) are calculated as shown in Table 11.

Table 9. The optimal values of design parameters obtained from MODE algorithm.

Design Parameter	A	B	C
Evaporator temperature (K)	278.3	281.3	279.1
Pump efficiency	0.79	0.84	0.87
Inlet pump temperature (K)	387	385	385
Evaporator pinch point temperature (K)	286.2	283.8	284.4
ORC turbine inlet pressure (Kpa)	1476	2038	3784
ORC turbine inlet temperature(K)	601	672.8	664.7
Turbine efficiency	0.82	0.88	0.91
Biomass flow rate (kg/s)	0.18	0.19	0.22

Table 10. Thermodynamic characteristics of three Pareto optimal solutions.

Parameter	A	B	C
$\dot{W}_{net}(kw)$	283.64	314.73	367.21
Ψ	0.29	0.31	0.34
$\dot{E}_{xD,tot}(kw)$	3783	3411	3496
$\dot{Q}_{Cooling}(kw)$	2065	1592	1626
$\dot{Q}_{Heating}(kw)$	1494	1773	1681
$\dot{C}_{tot}(\$/h)$	285.4	293.8	883.2
$\dot{m}_{Hot.W}(kg/s)$	0.56	0.58	0.55
CO_2(kg/Mwh)	351.3	374.8	369.7
$\dot{m}_{fresh}(kg/s)$	1.12	1.36	1.82

Table 11. The effects of design parameters on objective functions.

	$\dot{m}_{biomass}$	$P_{in,ORC,Turbin}$	$T_{in,ORC,Turbin}$	$T_{P,Evap}$	$\eta_{isen,Tur}$	T_{Evap}	$\eta_{isen,Pump}$
EE	Negative	Positive	Positive	Negative	Positive	Positive	NSE
TCR	Negative	Negative	Negative	Positive	Negative	Negative	NSE

NSE: No significant effect, EF: Exergy efficiency, TCR: Total cost rate ($/h)

The following conclusions can be made from Table 11:

An increase in the biomass flow rate has a negative effect on both objective functions. An increase in the biomass flow rate leads to a decrease in the system exergy efficiency because the denominator of exergy equation (Eq.(39)) increases. Furthermore, the negative impact on the total cost rate is a result of an increase in this parameter, which increases the total cost rate of the system.

When the ORC turbine inlet pressure increases, the total cost rate as well as the exergy efficiency increases. When the turbine inlet pressure increases due to an increase in the cooling load and the net power output of the system, the exergy efficiency of the system increases. When the inlet pressure as well as the turbine purchase cost increase, the total cost rate of the system is increased. As a result, an increase in the ORC turbine inlet pressure has a negative as well as positive effect on the objective functions.

An increase in turbine inlet temperature has a positive impact on the exergy efficiency because increasing the turbine inlet temperature has a positive and a negative impact on the objective function; while the other parameters are kept fixed, increasing this parameters leads to an increase in the turbine inlet enthalpy as well as turbine work, which finally results in an increase in exergy efficiency, according to Eq. (39). On the other hand, an increase in the turbine inlet temperature increases the total cost of the system due to an increase in the turbine purchase cost. An increase in the turbine purchase cost leads to an increase in the total cost of the system.

When the evaporator pinch point temperature increases, the exergy efficiency of the system decreases; this is a result of the fact that the higher the pinch point temperature, the lower the energy being utilized in evaporator; this leads to a reduction of the ORC turbine power output. On the other hand, an increase in the pinch point temperature, while fixing other design parameters, results in a decrease in the heat transfer area of the evaporator. This is why the total cost rate of the system decreases.

An increase in the isentropic turbine efficiency results in an increase in system exergy efficiency and an increase in the total cost of the system. Increasing this parameter results in an increase in the steam turbine power output; this directly leads to an increase in exergy efficiency. Moreover, increasing this parameter leads to an increase in steam turbine purchase and maintenance cost.

Increasing the absorption chiller evaporator temperature results in an increase in the cooling load of the absorption chiller and simultaneously increases the cost of the chiller. The other parameter, pump isentropic efficiency, does not have a significant effect on any of the objective functions. The reason behind this phenomenon is that unlike the maintenance and the purchase cost of the turbine, the purchase cost of pumps is relatively low.

The system under study is compared to a multigeneration energy system from various

aspects such as thermodynamic modeling, environmental impact, and exergy analysis. Products of each energy system are shown in Table 12.

System 1 consists of a gas turbine cycle, an organic Rankine cycle (ORC), a single-effect absorption chiller, a domestic water heater, and a PEM electrolyzer [51]. According to the results presented in Table 12, it is observed that the net power output of System 2 (i.e., the system studied in this paper) is lower than System 1. However, the total cost rate as well as the CO_2 emission of System 2 is lower than System 1.

In order to select one of these two systems as the final choice, one should prioritize the requirement first. For example, if CO_2 emission or the total cost is the priority, then, System 2 is the most suitable system. In addition, the place where the system is going to be used should have adequate biomass. However, the amount of each useful output can help designers to decide on which system is to be selected. For instance, the gas turbine multigeneration system can provide more electricity than a biomass-based energy system.

From the above comparison, it is concluded that several factors may impact the decisions on selecting a suitable multigeneration energy system. These factors include system cost, product requirement (e.g., electricity, heating, cooling, etc.), environmental impact, multigeneration site location, fuel availability, and cost.

8. Conclusion

In this paper, the thermodynamic, exergy, and exergy economic modeling of a multigeneration energy system were presented. The optimal design of the mentioned energy system was performed using a hybrid evolutionary algorithm based on MODE and the LUS technique. Then, the results were compared with the MOPSO and the NSGA-II methods. The effectiveness and the advantages of the proposed method were verified using various indices. In order to provide a closed form equation for the system, a curve-fitting technique was applied on the obtained optimized points. Furthermore, the effects of the different design parameters on the total cost rate and exergy efficiency were evaluated using sensitivity analysis.

References

[1] Zhang L., Xu C.C., Champagne P., Overview of Recent Advances in Thermo-chemical Conversion of Biomass, Energy Conversion and Management. (2010)51(5):969-82.

[2] Dong Y., Steinberg M., Hynol an Aconomical Process for Methanol Production from Biomass and Natural Gas with Reduced CO2 Emission, International Journal of Hydrogen Energy (1997) 22(10-11):971-7.

[3] Ahmadi P., Dincer I., Rosen M.A., Thermoeconomic Multi-Objective Optimization of a Novel Biomass-Based Integrated Energy System, Energy (2014) 68:958-70.

[4] Ahmadi P., Dincer I., Rosen M.A., Development and Assessment of an Integrated Biomass-Based Multigeneration Energy System, Energy (2013)56:155-66.

[5] Wang J., Yang Y., Energy, Exergy and Environmental Analysis of a Hybrid Combined Cooling Heating and Power System Utilizing Biomass and Solar Energy, Energy Conversion and Management (2016)124:566-77.

[6] Salemme L., Simeone M., Chirone R., Salatino P., Analysis of the Energy Efficiency of Solar Aided Biomass Gasification for Pure Hydrogen Production, International Journal of Hydrogen energy (2014) 39(27):14622-32.

[7] Nakyai T., Authayanun S., Patcharavorachot Y., Arpornwichanop A., Assabumrungrat S., Saebea D., Exergoeconomics of Hydrogen Production from Biomass Air-Steam Gasification with Methane co-Feeding, Energy Conversion and Management. (2017)140:228-39.

[8] Wang J.J., Xu Z.L., Jin H.G., Shi G.H., Fu C., Yang K., Design Optimization and Analysis of a Biomass Gasification Based

Table 12. Comparison of two different multigeneration energy systems.

Parameters	$\dot{W}_{net}$ (kW)	Ψ	$\dot{Q}_{Cooling}$ (kW)	$\dot{Q}_{heating}$ (kW)	$\dot{C}_{tot}$ $(\$/h)$	CO_2 (kg/kWh)	$\dot{m}_{Hot,w}$ (kg/h)	$\dot{m}_{fresh}$ (kg/h)	$\dot{m}_{H_2}(\frac{kg}{h})$
System 1 [51]	10304	60.42	929.95	4858.95	592.61	136.94	2983	NA	0.71
System 2	314.73	0.31	1592	1773	293.8	0.374	2088	4896	NA

NA: Not available

BCHP System: A case Study in Harbin, China, Renewable Energy (2014)71:572-83.
[9] Maraver D., Sin A., Royo J., Sebastián F., Assessment of CCHP Systems Based on Biomass Combustion for Small-Scale Applications Through a Review of the Technology and Analysis of Energy Efficiency Parameters, Applied Energy (2013)102:1303-13.
[10] Gholamian E., Zare V., Mousavi S.M., Integration of Biomass Gasification with a Solid Oxide Fuel Cell in a Combined Cooling, Heating and Power System: A Thermodynamic and Environmental Analysis, International Journal of Hydrogen Energy (2016)41(44):20396-406.
[11] Fernandes A., Woudstra T., Aravind P.V., System Simulation and Exergy Analysis on the Use of Biomass-Derived Liquid-Hydrogen for SOFC/GT Powered Aircraft, International Journal of Hydrogen Energy (2015) 40(13):4683-97.
[12] Seyitoglu S.S., Dincer I., Kilicarslan A., Energy and Exergy Analyses of Hydrogen Production by Coal Gasification, International Journal of Hydrogen Energy (2017)42(4):2592-600.
[13] Kalinci Y., Dincer I., Hepbasli A., Energy and Exergy Analyses of a Hybrid Hydrogen Energy System: A Case Study for Bozcaada, International Journal of Hydrogen Energy (2017)42(4):2492-503.
[14] Borji M., Atashkari K., Ghorbani S., Nariman-Zadeh N., Parametric Analysis and Pareto Optimization of an Integrated Autothermal Biomass Gasification, Solid Oxide Fuel Cell and Micro Gas Turbine CHP System, International Journal of Hydrogen Energy (2015)40(41):14202-23.
[15] Kalinci Y., Hepbasli A., Dincer I., Exergoeconomic Analysis of Hydrogen Production from Biomass Gasification, International Journal of Hydrogen Energy (2012)37(21):16402-11.
[16] El-Emam R.S., Dincer I., Thermal Modeling and Efficiency Assessment of an Integrated Biomass Gasification and Solid Oxide Fuel Cell System, International Journal of Hydrogen Energy (2015)40(24):7694-706.
[17] Ramadan M., Khaled M., Ramadan H.S., Becherif M., Modeling and Sizing of Combined Fuel Cell-Thermal Solar System for Energy Generation, International Journal of Hydrogen Energy (2016) 41(44):19929-35.
[18] Khalid F., Dincer I., Rosen M.A., Techno-Economic Assessment of a Solar-Geothermal Multigeneration System for Buildings, International Journal of Hydrogen Energy (2017) 42(33): 21454-21462.
[19] Yuksel Y.E., Ozturk M., Thermodynamic and Thermoeconomic Analyses of a Geothermal Energy Based Integrated System for Hydrogen Production, International Journal of Hydrogen Energy (2017) 42(4):2530-46.
[20] Eveloy V., Karunkeyoon W., Rodgers P., Al Alili A., Energy, Exergy and Economic Analysis of an Integrated Solid Oxide Fuel Cell–Gas Turbine–Organic Rankine Power Generation System, International Journal of Hydrogen Energy (2016)41(31):13843-58.
[21] Alhayek B, Agelin-Chaab M, Reddy B., Analysis of an Innovative Direct Steam Generation-Based Parabolic Trough Collector Plant Hybridized with a Biomass Boiler, International Journal of Energy Research (2017) DOI: 10.1002/er.3785.
[22] Ozcan H., Dincer I., Performance Evaluation of an SOFC Based Trigeneration System Using Various Gaseous Fuels from Biomass Gasification, International Journal of Hydrogen Energy (2015) 40(24):7798-807.
[23] Hosseinpour S., Aghbashlo M., Tabatabaei M., Younesi H., Mehrpooya M., Ramakrishna S., Multi-Objective Exergy-Based Optimization of a Continuous Photobioreactor Applied to Produce Hydrogen Using a Novel Combination of Soft Computing Techniques, International Journal of Hydrogen Energy (2017)42(12):8518-29.
[24] Khanmohammadi S., Heidarnejad P., Javani N., Ganjehsarabi H., Exergoeconomic Analysis and Multi Objective Optimization of a Solar Based Integrated Energy System for Hydrogen Production, International Journal of Hydrogen Energy (2017)42(33): 21443-21453.
[25] Ziapour B.M., Hashtroudi A., Performance Study of an Enhanced Solar Greenhouse Combined with the Phase Change Material Using Genetic Algorithm Optimization Method, Applied Thermal Engineering (2017)110:253-64.
[26] Rabbani M., Mohammadi S., Mobini M., Optimum Design of a CCHP System Based on Economical, Energy and Environmental Considerations Using GA and PSO, International Journal of Industrial Engineering Computations (2018) 9(1):99-122.
[27] Ahmadi P., Dincer I., Rosen M.A., Multi-Objective Optimization of an Ocean Thermal Energy Conversion System for Hydrogen Production, International Journal of Hydrogen Energy (2015)40(24):7601-8.
[28] Shamoushaki M., Ghanatir F., Ehyaei M.A., Ahmadi A., Exergy and Exergoeconomic Analysis and Multi-Objective Optimisation of Gas Turbine Power Plant by Evolutionary Algorithms, Case study, Aliabad Katoul Power Plant, International Journal of Exergy (2017)22(3):279-307.
[29] Rahdar M.H., Heidari M., Ataei A., Choi J.K., Modeling and Optimization of R-717 and R-134a Ice Thermal Energy Storage Air Conditioning Systems Using NSGA-II and MOPSO Algorithms, Applied Thermal Engineering (2016) 96:217-27.
[30] Soheyli S., Mayam M.H., Mehrjoo M., Modeling a Novel CCHP System Including Solar and Wind Renewable Energy Resources and

Sizing by a CC-MOPSO Algorithm, Applied Energy (2016)184:375-95.
[31]Karellas S., Braimakis K., Energy–Exergy Analysis and Economic Investigation of a Cogeneration and Trigeneration ORC–VCC Hybrid System Utilizing Biomass Fuel and Solar Power, Energy Conversion and Management (2016)107:103-13.
[32]Ahmadi P., Dincer I., Rosen M.A., Energy and Exergy Analyses of Hydrogen Production via Solar-Boosted Ocean Thermal Energy Conversion and PEM Electrolysis, International Journal of Hydrogen Energy (2013) 38(4):1795-805.
[33]Rashidi F., Optimal Allocation of Plug-in Electric Vehicle Capacity to Produce Active, Reactive and Distorted Powers Using Differential Evolution Based Artificial Bee Colony Algorithm. IET Science, Measurement & Technology (2017) DOI: 10.1049/iet-smt.2016.0444.
[34]Das S., Suganthan P.N., Differential Evolution: A Survey of the State-of-the-Art, IEEE Transactions on Evolutionary Computation (2011)15(1):4-31.
[35]Gonuguntla V., Mallipeddi R., Veluvolu K.C., Differential Evolution with Population and Strategy Parameter Adaptation, Mathematical Problems in Engineering (2015)10.
[36]Neto J.X., Reynoso-Meza G., Ruppel T.H., Mariani V.C., dos Santos Coelho L., Solving non-Smooth Economic Dispatch by a New Combination of Continuous GRASP Algorithm and Differential Evolution, International Journal of Electrical Power & Energy Systems (2017) 84:13-24.
[37]ElQuliti S.A., Mohamed A.W., A Large-Scale Nonlinear Mixed-Binary Goal Programming Model to Assess Candidate Locations for Solar Energy Stations: An Improved Real-Binary Differential Evolution Algorithm with a Case Study. Journal of Computational and Theoretical Nanoscience (2016)13(11):7909-21.
[38]Rashidi F., Abiri E., Niknam T., Salehi M.R., On-line Parameter Identification of Power Plant Characteristics Based on Phasor Measurement unit Recorded Data Using Differential Evolution and bat Inspired Algorithm, IET Science, Measurement & Technology (2015)9(3):376-92.
[39]Noman N., Iba H., Differential Evolution for Economic Load Dispatch Problems, Electric Power Systems Research (2008)78(8):1322-31.
[40]Pedersen M.E., Chipperfield A.J., Simplifying Particle Swarm Optimization, Applied Soft Computing (2010)10(2):618-28.
[41]Sahu B.K., Pati T.K., Nayak J.R., Panda S., Kar S.K., A Novel Hybrid LUS–TLBO Optimized Fuzzy-PID Controller for Load Frequency Control of Multi-Source Power System, International Journal of Electrical Power & Energy Systems (2016)74:58-69.
[42]Mohanty P.K., Sahu B.K., Panda S., Tuning and Assessment of Proportional–Integral–Derivative Controller for an Automatic Voltage Regulator System Employing Local Unimodal Sampling Algorithm, Electric Power Components and Systems (2014) 42(9):959-69.
[43]Jung J., Song S., Hur K.B., Numerical Study on the Effects of Intake Valve Timing on Performance of a Natural Gas-Diesel Dual-Fuel Engine and Multi-Objective Pareto Optimization, Applied Thermal Engineering (2017)121:604-16.
[44]Raja B.D., Jhala R.L., Patel V., Many-Objective Optimization of Cross-Flow Plate-Fin Heat Exchanger, International Journal of Thermal Sciences (2017) 118:320-39.
[45]Gong W., Cai Z., An Improved Multiobjective Differential Evolution Based on Pareto-Adaptive ϵ-Dominance and Orthogonal Design, European Journal of Operational Research (2009)198(2):576-601.
[46]Deb K., Pratap A., Agarwal S., Meyarivan TA. A Fast and Elitist Multiobjective Genetic Algorithm: NSGA-II. IEEE Transactions on Evolutionary Computation (2002)6(2):182-97.
[47]Coello C.A., Pulido G.T., Lechuga M.S., Handling Multiple Objectives with Particle Swarm Optimization, IEEE Transactions on Evolutionary Computation (2004)8(3):256-79
[48]Jayah T.H., Aye L., Fuller R.J., Stewart D.F., Computer Simulation of a Downdraft Wood Gasifier for Tea Drying, Biomass and Bioenergy (2003)25(4):459-69.
[49]Jarungthammachote S., Dutta A., Thermodynamic Equilibrium Model and Second Law Analysis of a Downdraft Waste Gasifier, Energy (2007)32(9):1660-9.
[50]Shabanpour-Haghighi A., Seifi A.R., Niknam T., A Modified Teaching–Learning Based Optimization for Multi-Objective Optimal Power Flow Problem, Energy Conversion and Management (2014)77:597-607.
[51]Ahmadi P., Dincer I., Rosen M.A., Thermodynamic Modeling and Multi-Objective Evolutionary-Based Optimization of a New Multigeneration Energy System, Energy Conversion and Management (2013)76:282-300.